An Extratropical Cyclone Atlas

A Tool for Illustrating Cyclone Structure and Evolution Characteristics

BY H. F. DACRE, M. K. HAWCROFT, M. A. STRINGER, AND K. I. HODGES

Extratropical cyclones play a significant role in determining the day-to-day weather conditions in many parts of the world through their associated wind and precipitation patterns. Their typical evolution characteristics are therefore of great interest to both educators and researchers of extratropical cyclone dynamics. The structure and evolution of extratropical cyclones, as viewed from the surface, was first described in a 1922 *Geofysiske Publikasjoner* article by Bjerknes and Solberg, who developed a conceptual model called the Norwegian cyclone model. Inconsistencies between observations and the Norwegian model have led to refinements of the model and to the development of new conceptual models such as that proposed by Shapiro and Keyser (1990). Detailed analysis of the structure and evolution of individual extratropical cyclones suggests that although there is no universal life cycle of extratropical cyclones, some general cyclone characteristics can be identified [see review paper by Ulbrich et al. (2009) and references therein]. For example, Browning and Roberts (1994) described the structural evolution of a moderately intense extratropical cyclone, using a combination of surface observations, satellite imagery, radar data, and model output. They identified and described the evolution of cyclonic flows, such as the warm and cold conveyor belt flows and the dry intrusion. Such case studies have contributed significantly to the generation of three-dimensional conceptual models of extratropical cyclones that provide a framework for understanding their dynamical evolution. These conceptual models are widely used in educational meteorology courses and texts throughout the world to illustrate the basic structure and evolution of extratropical cyclones.

The aim of this article is to go beyond individual case study analysis and introduce and promote the use of a comprehensive set of quantitative analyses describing the structure and evolution characteristics of 200 composited North Atlantic cyclones from 1989 to 2009. It is hoped that both teachers and researchers of extratropical cyclone dynamics will make use of the analyzed fields in the atlas, which is freely available via the storms project website (www.met.rdg.ac.uk/~storms). Some examples of how this atlas could be used for teaching are provided in the summary.

The atlas has been created to explore the mean structure and evolution of the 200 most intense North Atlantic cyclones identified in 20 winters of the ERA-Interim reanalysis data. The method used to create the composite fields is described in section 2. In sections 3 and 4, vertical and horizontal composites of cyclone structure for cyclones generated in the North Atlantic regions are used to subjectively identify features such as the relative positions of cold, warm, and occluded fronts and their associated wind and cloud patterns. Section 5 illustrates the evolution of cyclonic flows such as the warm and cold conveyor belts and dry intrusion. A summary is presented in section 6.

CREATING THE ATLAS. Following the work by Catto et al. in a 2010 *Journal of Climate* article, we applied an objective feature-tracking algorithm to fields from the European Centre for Medium Range Weather Forecasts' (ECMWF) ERA-Interim reanalysis for the winter period (December–February) of the years 1989–2009. Reanalysis data provide

AFFILIATIONS: DACRE, HAWCROFT, AND STRINGER—Department of Meteorology, University of Reading, Reading, United Kingdom; HODGES—National Centre for Earth Observation, Reading, United Kingdom
CORRESPONDING AUTHOR: H. F. Dacre, Department of Meteorology, University of Reading, Earley Gate, P.O. Box 243, Reading, RG6 6BB United Kingdom
E-mail: h.f.dacre@reading.ac.uk

DOI:10.1175/BAMS-D-11-00164.1

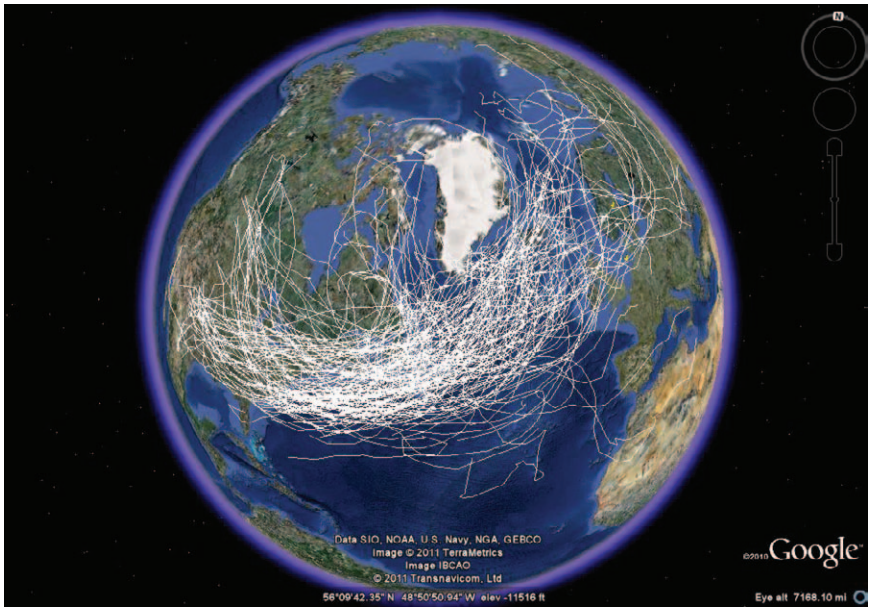

Fig. 1. Tracks of the 200 most intense winter cyclone tracks with maximum intensity, in terms of T42 vorticity, in the North Atlantic (white lines). (Image: Google Earth)

a spatially complete and coherent record of the global atmospheric circulation. Unlike archived weather analyses from operational forecasting systems, a reanalysis is produced with a single version of a data assimilation system, and is therefore not affected by changes in method. The temporal resolution of the data is 6 hourly. Tracks are identified using the 850-hPa relative vorticity truncated to T42 resolution to emphasize the synoptic scales. The 850-hPa relative vorticity features have been filtered to remove stationary or short-lived features that are not associated with extratropical cyclones. Figure 1 shows the 200 most intense—in terms of the T42 vorticity—winter cyclone tracks with maximum intensity in the North Atlantic (70°–10°W, 30°–90°N) that are used in the composites. Of the total 1,050 North Atlantic cyclones identified, the cyclone composites in the extratropical cyclone database represent only the most extreme cyclones (~19% of the entire North Atlantic cyclone distribution).

The required fields (e.g., relative humidity, temperature, geopotential height) are extracted from the ERA-Interim dataset along the tracks of the selected cyclones within a 20° radius surrounding the identified cyclone position on constant pressure surfaces or on constant potential temperature (θ) surfaces. The composites are produced by identifying the required offset time relative to the time of maximum intensity of each cyclone and the corresponding fields on the radial grid, averaged. Individual case studies often include mesoscale detail that masks the coherent features of cyclone development, whereas composites can highlight persistent

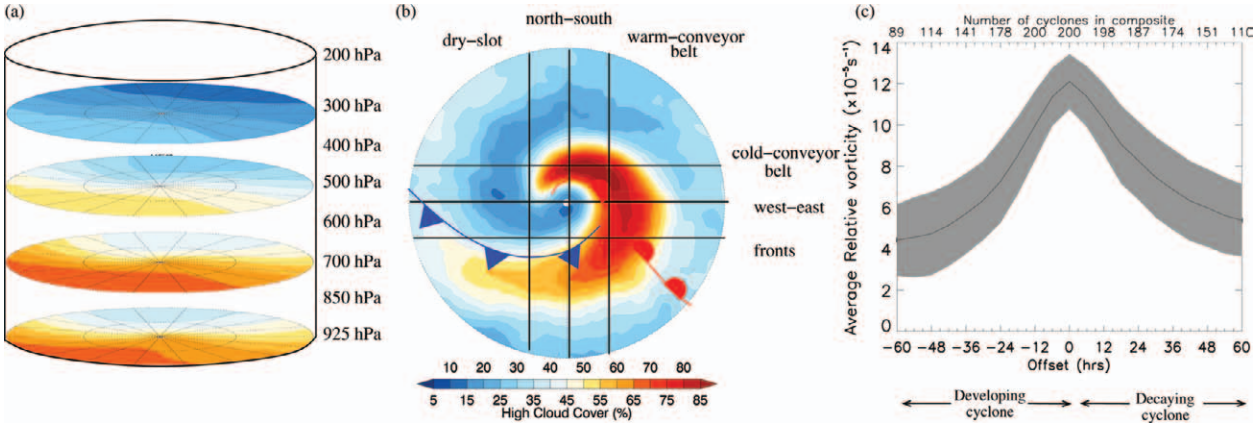

Fig. 2. Extratropical cyclone atlas options for selecting composite fields (a) on pressure surfaces; (b) along vertical cross sections; and (c) at different times in the cyclone life cycle relative to the time of maximum 850-hPa relative vorticity (shading represents ± 1 standard deviation).

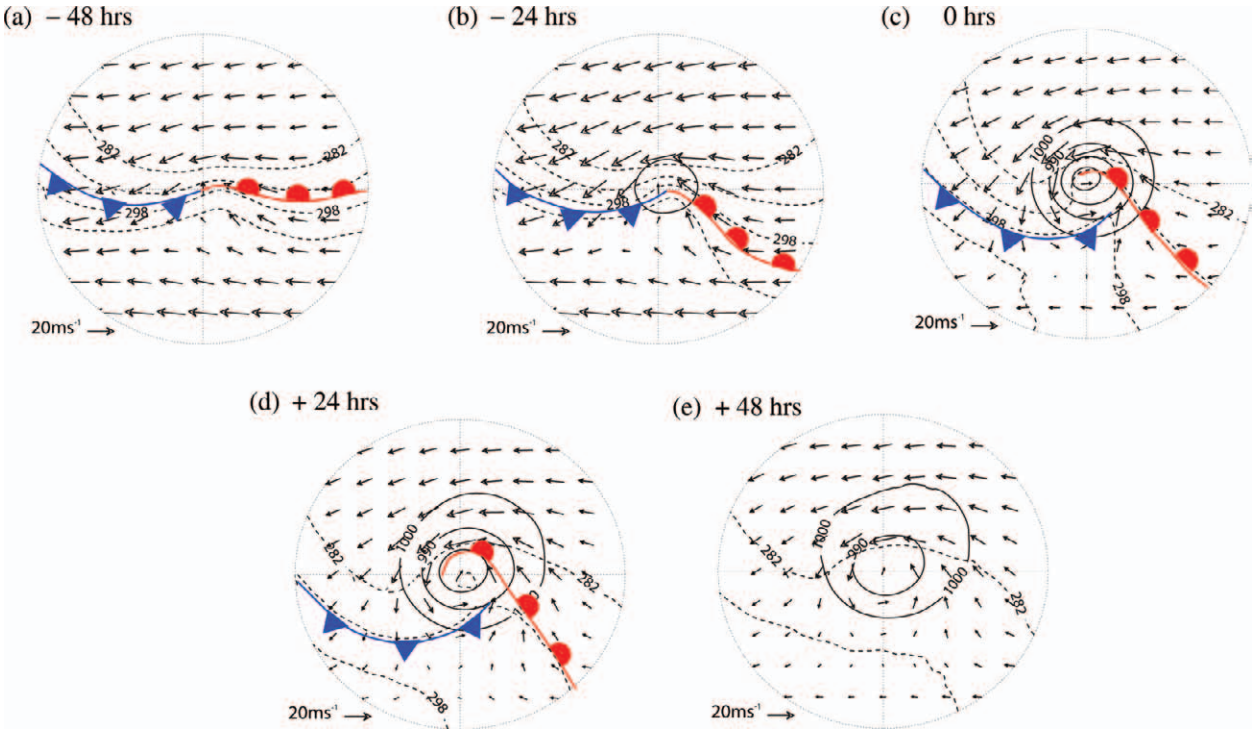

FIG. 3. Horizontal composites from the extratropical cyclone atlas show the position of 925-hPa fronts, closed MSLP contours (solid lines at 10-hPa intervals), 925-hPa system-relative wind vectors, and 925-hPa equivalent potential temperature (θ_e, dashed lines at 282, 290, and 298 K) at (a) 48 and (b) 24 h before maximum intensity; (c) at the time of maximum intensity; and (d) 24 and (e) 48 h after maximum intensity.

basic features of cyclone evolution. Note, however, that composites can blur important mesoscale detail such as frontal boundaries, especially at locations distant from the cyclone center. Uncertainty in the composite fields can be represented by the standard deviation among the composite members. A full description of the compositing method is given on the website (www.met.rdg.ac.uk/~storms/method).

The Web version of the extratropical cyclone atlas contains composites that can be selected on pressure surfaces (Fig. 2a); on θ surfaces (265, 275, 285, 300, 315, 330, 350, and 395 K) or on a single level (e.g., mean sea level pressure and cloud cover). Also available are vertical cross sections through different features of the cyclone (Fig. 2b). Both horizontal and vertical composite slices are included in the atlas and can be viewed at different stages in the cyclone life cycle by selecting times relative to the time of maximum cyclone intensity (Fig. 2c). Note that care should be taken when comparing composites at different stages in the cyclone life cycle, as the composites at each stage include a different number of cyclones. The number of cyclones in each composite is shown in Fig. 2c.

EVOLUTION OF THE LOW-LEVEL CYCLONE. Low-level fields from the extratropical cyclone atlas have been combined to create diagrams of low-level cyclone structure and evolution that are comparable to the conceptual models described by Bjerknes and Solberg (1922) and Shapiro and Keyser (1990).

Figure 3 shows composites of low-level fields throughout the developing and decaying stages of the composite cyclone life cycle. During the developing stage (Figs. 3a and b), the low-level temperature wave (denoted by equivalent potential temperature, θ_e) can be seen to amplify as a wedge of warm, moist air between the cold and warm fronts, known as the warm sector, develops. At the same time, development of a closed isobar forms and the central pressure falls; cyclonic circulation and system-relative wind speeds around the cyclone center increase. The system-relative winds are computed by subtracting the propagation speed of the cyclone from the gridded winds for each individual cyclone before compositing. The propagation speed is computed as the great circle distance between two track points divided by the time step (6 h). At the time of maximum intensity

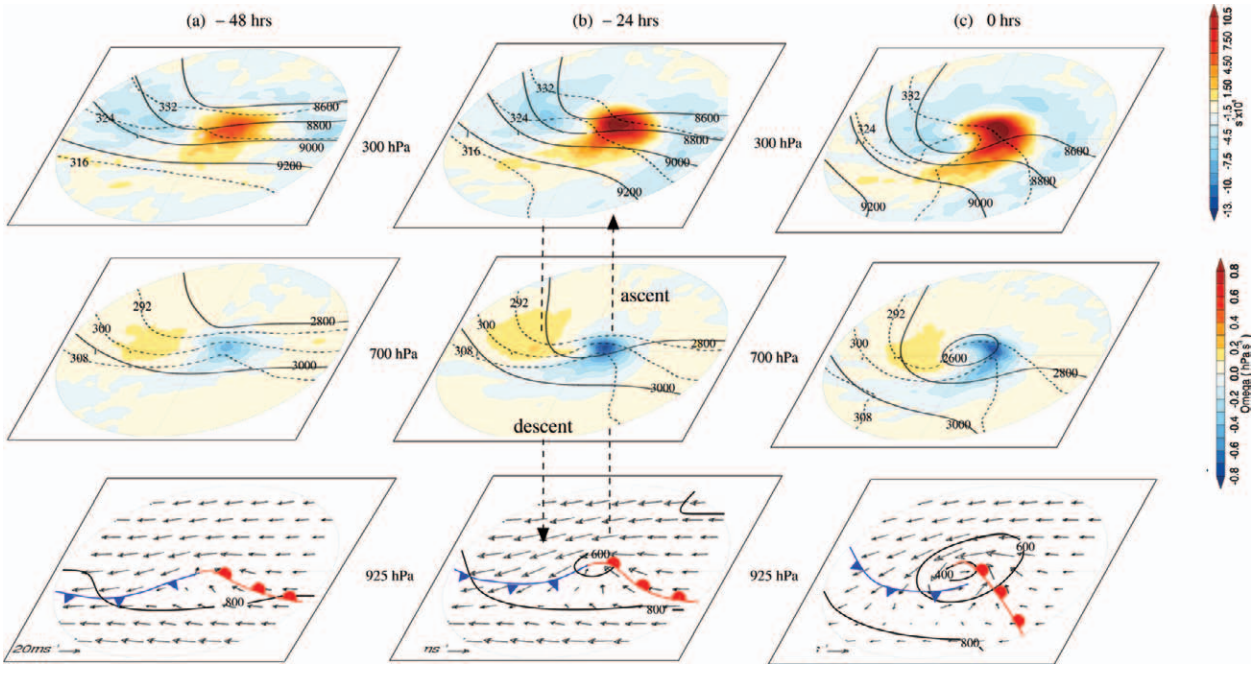

Fig. 4. Horizontal composites at (a) 48 and (b) 24 h before the time of maximum intensity, and (c) at the time of maximum intensity. Bottom row: 925-hPa geopotential height (solid lines at 400, 600, and 800 m); system-relative wind vectors, and frontal positions. Middle row: 700-hPa geopotential height (solid lines at 2,800 and 3,000 m); equivalent potential temperature (θ_e, dashed lines at 292, 300, and 308 K) and vertical velocity (Omega, filled). Top row: 300-hPa geopotential height (solid lines at 8,600, 8,800, 9,000, and 9,200 m); θ_e (dashed lines at 316, 324, and 332 K) and divergence (filled).

(Fig. 3c), the lowest central pressure occurs and the tight pressure gradient results in peak wind speeds. During the first 24 hours of the decaying stage of the cyclone lifecycle (Fig. 3d), the central pressure increases and pressure gradients decrease, leading to lower wind speeds; the low-level fronts weaken and the warm front wraps around the cyclone center. Between 24 and 48 hours after maximum intensity (Fig. 3e), the central pressure continues to rise and the frontal gradients weaken further.

EVOLUTION OF THE VERTICAL CYCLONE STRUCTURE. Composites of lower- and upper-level fields throughout the developing stage of the composite cyclone life cycle have been combined to illustrate the relative development of the cyclone at upper and lower levels. These figures are comparable to the conceptual models described in Semple (2003) and Browning (1990), etc.

In the initial stage of development (Fig. 4a), a weak low-level temperature wave is seen to form downstream of an upper-level shortwave trough. As the surface cyclone develops (Figs. 4b,c), cold air advection to the west of the surface cyclone reduces the thickness of the atmospheric layer between 1,000 and 500 hPa and deepens the upper-level trough. Conversely, warm air advection to the east of the surface cyclone increases the 1,000–500-hPa thickness and intensifies the upper-level ridge. Thus, differential temperature advection to the west and east of the surface cyclone amplifies the upper-level wave.

As the upper-level wave amplifies, positive differential vorticity advection downstream of the upper-level trough forces ascent above the surface cyclone. The resulting lower-tropospheric vortex stretching intensifies the surface cyclone. Increased low-level wind speeds lead to an amplification of the low-level temperature wave and hence stronger low-level temperature advection, which in turn amplifies the upper-level wave. Therefore, a positive feedback occurs between the processes occurring at upper and lower-levels.

As the cyclone develops, the upper-level low-pressure region moves toward the surface low. In the mature stage, the upper-level low is located directly above the surface low, producing a vertically stacked

cold-core system. The alignment of the surface and upper-level cyclones means that there is no longer a positive feedback effect between the processes occurring at upper and lower levels, and the cyclone decays (not shown).

IDENTIFYING AIR FLOWS WITHIN EXTRATROPICAL CYCLONES. In this section, the main airflows—namely, the warm and cold conveyor belts and dry intrusion—are subjectively identified at the time of maximum intensity by analyzing system-relative flow on isentropic surfaces.

At the time of maximum intensity, a region of high cloud cover can be seen wrapping cyclonically around the low pressure center (Fig. 5b), associated with the warm conveyor belt (WCB). The warm conveyor belt is a warm, moist synoptic-scale flow of air that advances poleward ahead of the cold front and then splits into two air flows. One air flow (WCB1) ascends along the axis of the cold front and then turns anticyclonically, broadening the polar front cloud band at upper levels. The second air flow (WCB2) peels off cyclonically from the warm conveyor belt and ascends to form the upper part of a cloud head, which emerges from the polar front cloud band. The cloud head is also enhanced by a flow of air coming from the cold conveyor belt. The cold conveyor belt is a flow of air characterized by lower temperatures that flows rearward, relative to the advancing system and ahead of the warm front, and ascends to form the lower part of the cloud head (Fig. 5a). Also identified is a cloud-free dry intrusion that penetrates into the frontal cloud, separating the emerging cloud head from the polar front cloud band to form a comma pattern (Fig. 5b). This dry intrusion is caused by a stream of dry air from the lower stratosphere descending through a tropopause fold, into the center of the cyclone. As the cyclone develops further, the cloud head wraps around the cyclone center and begins to dissipate (not shown).

Figure 5c shows a vertical composite plot along the warm conveyor belt transect in Fig. 2b. The θ_e contours are vertically inclined, rising from the warm sector to the south of the cyclone and northward over the surface warm front. The region of maximum ascent and highest relative humidity is found close to the cyclone center between the 285- and 300-K θ_e surfaces. The cold conveyor belt flow is identified behind the surface warm front flowing rearward relative to the propagation direction of the cyclone.

SUMMARY. Composites of extratropical cyclone structure and evolution have been created by compositing data surrounding the 200 most intense North Atlantic winter cyclones in the ERA-Interim reanalysis dataset. The composite structures are consistent

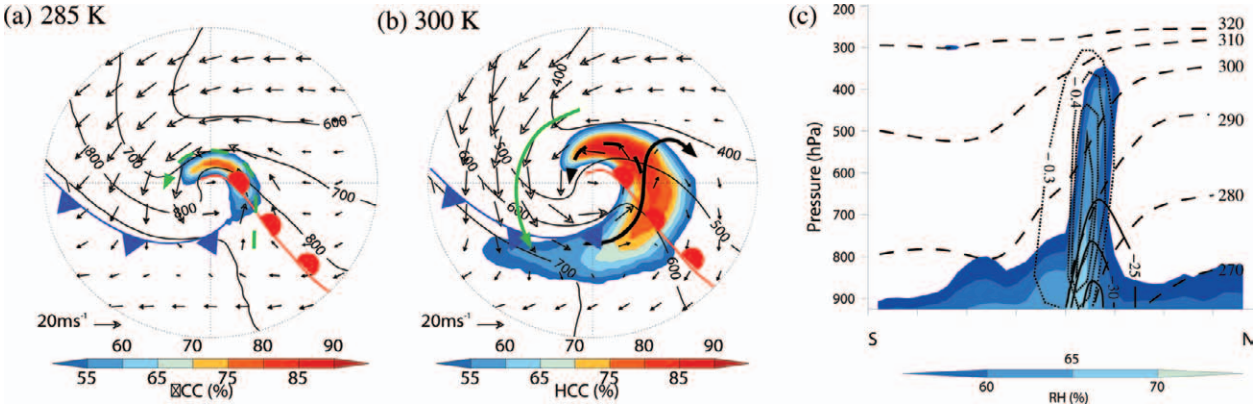

Fig. 5. Horizontal composites at the time of maximum intensity. (a) Pressure (solid lines at 900, 800, 700, and 600 hPa) and system-relative wind vectors on a 285-K isentropic surface; midlevel cloud cover (MCC; filled, >50%); and overlaid surface fronts. Bold green dashed arrow indicates a cold conveyor belt flow. (b) Pressure (solid lines at 700, 600, 500, and 400 hPa) and system-relative wind vectors on a 300-K isentropic surface; high-level cloud cover (HCC; filled, >50%); and overlaid surface fronts. Bold arrows indicate warm conveyor belt (WCB) flows (WCB1: solid black line; WCB2: dashed black line) and a dry air intrusion (solid green). (c) Vertical cross section along the WCB transect (Fig. 2b). Contours are system-relative u-component of the wind (solid lines at −35, −30, and −25 m s^{-1}); equivalent potential temperature (θ_e, dashed lines from 270 to 320 K), vertical velocity (dotted lines, at −0.6, −0.5, −0.4, and −0.3 hPa s^{-1}); and relative humidity (RH; filled, >55%).

with conceptual diagrams based on individual case studies. Features such as frontal positions and their associated wind and cloud patterns are analyzed along with the evolution of cyclonic flows such as the warm and cold conveyor belts and dry intrusions. These features are illustrated in this article using composite conceptual diagrams that are available for educational and research purposes from the storms project website (www.met.rdg.ac.uk/~storms). A wide range of diagnostics is available on the website, which contains an atlas of horizontally composited fields on pressure surfaces and potential temperature surfaces as well as vertically composited fields taken through features in the cyclone such as the dry intrusion and warm and cold fronts.

Some examples of how this atlas could be used for both educational and research purposes include

- providing *quantitative* values for atmospheric variables associated with "typical" extratropical cyclones (e.g., frontal temperature gradients, jet streak wind speeds, ascent and descent rates);
- introducing students to the concept of system-relative winds;
- teaching students about flow along isentropic surfaces;
- teaching students how to position surface fronts; and
- comparison of average fields with case study analysis.

ACKNOWLEDGMENTS. We are grateful to Jennifer Catto at Monash University, for allowing us to use her composite plotting scripts, and to Sue Gray at the University of Reading, for helpful comments on the manuscript. Marc Stringer was supported by a NERC small grant, and Matt Hawcroft is supported on the NERC-funded TEMPEST project.

FOR FURTHER READING

Ahrens, C. D., 2000: *Meteorology Today: An Introduction to Weather, Climate, and the Environment.* Brooks/Cole, 528 pp.

Bjerknes, J., and H. Solberg, 1922: Life cycle of cyclones and the polar front theory of atmospheric circulation. *Geofys. Publ.,* **3,** 1–18.

Browning, K. A., 1990: Organisation of clouds and precipitation in extratropical cyclones. *Extratropical Cyclones; The Erik Palmén Memorial Volume,* C. W. Newton and E. O. Holopainen, Eds., 129–153.

——, and N. M. Roberts, 1994: Structure of a frontal cyclone. *Quart. J. Roy. Meteor. Soc.*, **120,** 1535–1557.

Carlson, T. N., 1980: Airflow through midlatitude cyclones and the comma cloud pattern. *Mon. Wea. Rev.,* **108,** 1498–1509.

Catto, J. L., L. C. Shaffrey, and K. L. Hodges, 2010: Can climate models capture the structure of extratropical cyclones? *J. Climate,* **23,** 1621–1635.

Dacre, H. F., and S. L. Gray, 2009: The spatial distribution and evolution characteristics of North Atlantic cyclones. *Mon. Wea. Rev.,* **137,** 99–115.

Harrold, T. W., 1973: Mechanisms influencing the distribution of precipitation within baroclinic disturbances. *Quart. J. Roy. Meteor. Soc.,* **99,** 232–251.

Hodges, K. I., 1995: Feature tracking on the unit sphere. *Mon. Wea. Rev.,* **123,** 3458–3465.

——, 1999: Adaptive constraints for feature tracking. *Mon. Wea. Rev.,* **127,** 1362–1373.

Petterssen, S., and S. J. Smebye, 1971: On the development of extratropical cyclones. *Quart. J. Roy. Meteor. Soc.,* **97,** 457–482.

Rudeva, I. A., and S. K. Gulev, 2011: Composite analysis of North Atlantic extratropical cyclones in NCEP/NCAR reanalysis data. *Mon. Wea. Rev.,* **139,** 1419–1436.

Semple, A. T., 2003: A review and unification of conceptual models of cyclogenesis. *Meteor. Appl.,* **10,** 39–59.

Shapiro, M. A., and D. Keyser, 1990: On the structure and dynamics of fronts, jet streams and the tropopause. *Extratropical Cyclones: The Erik Palmén Memorial Volume,* C. W. Newton and E. O. Holopainen, Eds., 167–191.

Simmons, A. J., S. Uppala, D. Dee, and S. Kobayashi, 2007: ERA-Interim: New ECMWF reanalysis products from 1989 onwards. *ECMWF Newsletter,* **110,** 25–35.

Sinclair, M. R., and M. J. Revell, 2000: Classification and composite diagnosis of extratropical cyclogenesis in the southwest Pacific. *Mon. Wea. Rev.,* **128,** 1089–1105.

Ulbrich, U., G. C. Leckebusch, and J. G. Pinto, 2009: Extra-tropical cyclones in the present and future climate: A review. *Theor. Appl. Climatol.,* **96,** 117–131, doi:10.1007/s00704-008-0083-8.

Young, M. V., G. A. Monk, and K. A. Browning, 1987: Interpretation of satellite imagery of a rapidly deepening cyclone. *Quart. J. Roy. Meteor. Soc.,* **113,** 1089–1115.